Acoustic design and analyses of a double Skin Façade system

Zhongyu Hu, Laurent Maxit, Li Cheng

Acoustic Design and Analyses of a Double Skin Façade System

Zhongyu HU[1], Laurent MAXIT[2], and Li CHENG[1*]

[1]Department of Mechanical Engineering, The Hong Kong Polytechnic University, Hung Hom, Kowloon, Hong Kong, China

[2]Laboratoire Vibrations Acoustique, INSA Lyon, 25 bis, avenue Jean Capelle, 69621 Villeurbanne Cedex, France

*Corresponding author: li.cheng@polyu.edu.hk

Abstract

Noise insulation in buildings is an important topic in building acoustics. Existing literature shows a clear lack of simulation tools for the design, analysis, and assessment of the sound insulation performance of building structures, especially when the frequency of interest becomes higher. To tackle this problem, a numerical based Condensed Transfer Function (CTF) method, alongside a piecewise calculation scheme, is adapted to investigate a simplified Double Skin Façade (DSF) system. Embracing a sub-structuring philosophy, the method offers an appealing alternative to existing analyses ones in terms of providing enhanced computational efficiency and enriched physical description of the system. Numerical analyses reveal dominant sound transmission paths into a typical receiving room. Meanwhile, as sound reduction devices, microperforated panels are investigated in two arrangements, triggering different sound absorption behaviors and design principles. The proposed model allows extensions to other building structures.

Keywords: building acoustics; numerical method; sound insulation; microperforated panel

1. Introduction

Noise insulation in buildings greatly affects the quality of living comfort, thus motivating persistent effort in developing innovative solutions. The history of building acoustics begins with the famous reverberation formula proposed by Sabine in the late 1890s. Since then, various prediction tools were developed, exemplified by methods based on geometrical acoustics, diffusion equation and wave propagation [1]. Geometrical methods and diffusion equation methods are highly descriptive and therefore frequently applied in a much-simplified form to increase the modeling efficiency in the high-frequency range [2, 3]. The former one, which is also referred to as ray acoustic methods, considers the fact that the sound travels along straight lines while the latter is energy-based which allows efficient prediction of the acoustic properties of a room such as reverberation time. By comparison, wave methods are developed based on the solutions of the wave equation, which are inevitably more computationally intensive. However, wave based methods generally offer better and more detailed physical descriptions of the system, more conducive to system design and optimization [4, 5].

To solve the wave equation, numerical tools used in traditional vibro-acoustics are generally applied, such as the Boundary Element Method (BEM) and Finite Element Method (FEM). For example, Arjunan *et al* developed a 2D FEM to predict the Sound Reduction Index (SRI) of a stud-based double leaf wall of finite size [6]. Despite the insightful analyses, it was recognized that the extension of the method to 3D analyses would be difficult due to the large number of elements needed. In fact, as a rule of thumb, at least 8 elements per wavelength are usually required to obtain converged and reliable results [6]. Transfer Matrix Method (TMM) is an efficient modeling tool to deal with the prediction of sound transmission in multilayer systems. Santoni *et al* [7] developed a numerical model based on the TMM to calculate the ratio of average velocity between two layers S_1 and S_2. The model shows good agreement with experimental data in the low-frequency range. Nevertheless, despite its effectiveness in dealing

with sound transmission problems, TMM method needs further improvement in terms of acoustic field prediction within the inner layer. Using a double leaf partition configuration, the Finite Layer Method (FLM) [8] shows improved computational efficiency. The FLM uses the modal decomposition technique to model the partition in the in-plane direction and the FEM in the perpendicular direction. However, when an opening is present in the partition, as in the case of a Double Skin Façade (DSF) system, the method fails. The so-called DSF design represents a new type of building structure, which gains increasing popularity due to the immense economic benefit it offers. A typical DSF consists of two parallel skins/panels arranged in such a way that the air can flow within the intermediate cavity, which enables a reduced energy consumption while allowing for natural ventilation. For the obvious thermal and energy benefit, the use of DSF in building design has been attracting increasing attention in the last two decades. While the thermal aspect has been adequately considered owing to the available analysis and design tools, it is not quite the case for noise consideration. A typical example among some useful attempts is the work of Urban *et al*. in which a simple model was established for the acoustic prediction of a naturally ventilated DSF structure with openings [9]. It is well accepted that one of the major problems of the DSF system is the increasing noise transmission into the building. However, most existing evaluations on the acoustic performances of façades and windows are based on relatively simple empirical formulae [10-13], which, despite their simplicity and usefulness, can hardly address the issue of parameter tuning and sophisticated optimization at the early design stage. Indeed, the noise insulation properties of a DSF system are highly dependent on numerous system parameters (material properties of skins, dimensions of cavities, size of apertures, possible uses of acoustic control devices, etc.). Meanwhile, the large size of the system and the wide frequency range to be considered both increase the modal density of the system, thus posing even harsher demand on the numerical tools.

Another challenge roots in the integration and the performance prediction of various noise mitigation measures into the modelling framework, exemplified by sound absorbing devices. Typical examples include porous materials [14-16] or Micro-Perforated Panels (MPP) targeting high frequencies and wide bandwidth [17-19] and Helmholtz Resonators targeting low frequencies and tonal noise [20-22]. Although extensive research on the acoustic properties of an individual device has been available, their inclusions in complex vibroacoustic systems, such as a DSF system, pose additional challenges. The unknowns are mainly in two aspects: 1) the need to model the coupling between the physical environment and the sound absorption devices; 2) the characterization of the in-situ performance of different sound absorption arrangements and the understanding of their physical mechanisms. While several experimental investigations on the noise insulation performance of building façades were conducted, existing numerical models are either time consuming or lack required finesse in terms of accuracy or the information provided. An ideal tool should be the one that can balance the required simulation accuracy and efficiency and provide flexibility as well as the wealth of information for a large DSF system over a broad frequency range.

The above analyses motivated the present research, which intends to offer its novelty through targeting a twofold-objective: 1) adapting a so-called Condensed Transfer Function (CTF) method and dealing with the aforementioned modelling challenges, mainly in the mid frequency range, in a typical DSF system, with MPP-based sound absorption devices integrated as a coupled component; and 2) analyzing noise transmission paths through the system and the *in-situ* sound absorption mechanisms of different sound absorption arrangements to explore possible ways to improve the noise insulation of a typical DSF design.

The CTF method has been developed for the modelling of complex vibroacoustic systems under a sub-structuring philosophy. The method embraces the principle of sub-structuring to push the computational limit through obtaining transfer functions of sub-system models before

system assembly. Transfer functions of uncoupled sub-systems can be calculated using different methods (analytical, numerical or even experimental). The method has been employed to study a wide range of mechanical problems [23-25]. Compared with FEM, the CTF method incurs a lower computational cost owing to its less demanding meshing criteria. As an important step of improvement, recent research proposed a piecewise calculation scheme for the mid-to-high frequency modelling [26]. It was shown that the computational efficiency could be further improved in weakly coupled systems when the interface functions can match the structure wave motions. The scheme was later extended to strongly coupled systems and experimentally validated [27].

This paper aims at adapting the CTF method and the piecewise scheme to accommodate the vibro-acoustic simulation of a typical DSF system and investigate the possible noise mitigation measures by using MPP-based acoustic treatment. After establishing the general modelling framework, numerical analyses are performed on a typical acoustic room coupled with a DSF system in terms of frequency responses, sound insulation performance, energy transmission path, as well as the physical mechanism of the MPPs. It is shown that the flexibility and the modularity of the proposed method suit particularly well the analysis and design needs of DSF systems, especially at the early design stage. For DSFs which fail to provide adequate acoustic insulation, integrating MPP absorptions, either in the form of wall treatment or a suspended curtain/screen, provides an efficient solution for noise mitigation, though with different absorption behavior and design principles. Numerical examples demonstrate that the proposed modeling methodology allows a fine and detailed description of the system with a relatively complex configuration and a large dimension in the mid frequency range.

2. Theoretical Model and Formulation

Consider a DSF system, comprising mainly a double glass glazing and an acoustic room, as shown in Fig. 1. Incident sound waves impinge upon the outer glass, which radiates sound into a space between the outer glass and the inner glass. This space is referred to as DSF cavity. The inner class contains a ventilation opening connecting the DSF cavity and a receiving room. Both glass panels are considered to be flexible. Therefore, acoustic energy can be transmitted into the room via both the inner glass and the ventilation opening. To increase the sound absorption inside the room, MPPs are installed in two different ways. As shown by the dotted lines in Fig. 1, option 1 is to use an MPP as a screen/curtain inside the DSF cavity, whilst option 2 has an MPP absorber (MPPA) installed as a sidewall on the room ceiling. For the latter, the MPPA comprises a sheet of MPP with a backing cavity, which is partitioned into small volumes to avoid the interactions among different holes [18]. Therefore, the MPPA is considered as locally reacting. All other walls of the room, as well as the sidewalls of the DSF cavity, are all assumed to be acoustically rigid. As a special case, when the MPPA is absent, the room ceiling becomes a rigid wall.

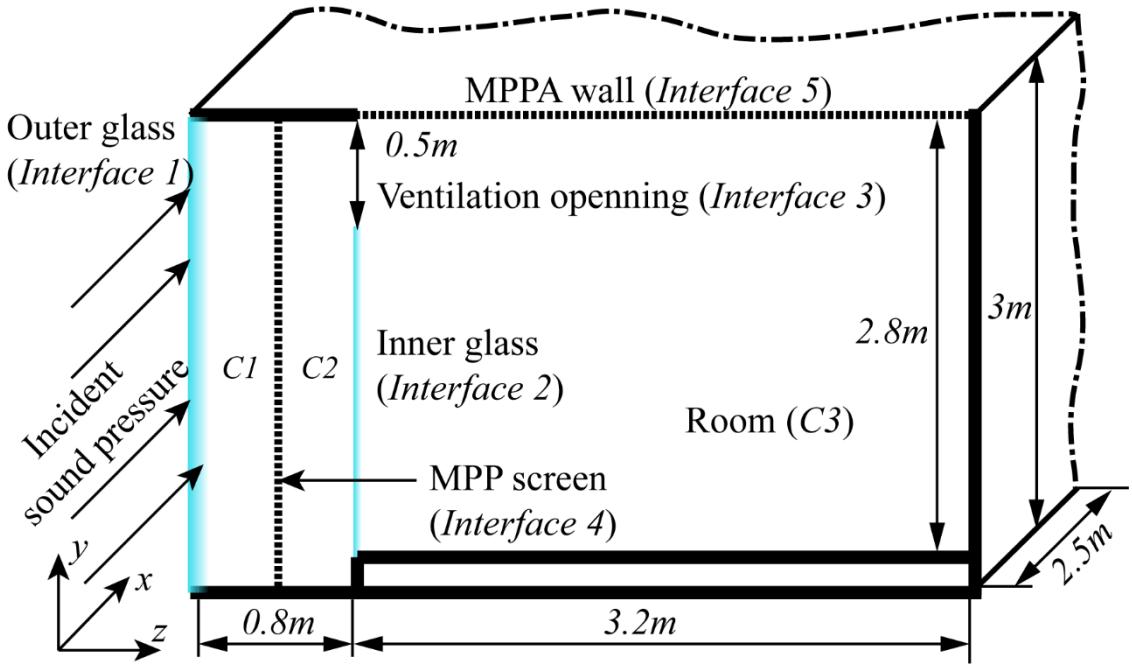

Figure 1 Configuration of the DSF system under investigation.

Several notations are annotated in Fig. 1, to be used in the formulation. The MPP screen divides the DSF cavity into two sub-cavities: C1 and C2. When the MPP is absent, the DSF cavity is denoted as C1 only. The acoustic room is denoted as C3. The outer glass, inner glass, and the ventilation opening are represented as interfaces 1, 2, and 3, respectively. The MPP screen and the locally reacting MPP wall are denoted as interfaces 4 and 5, respectively.

It can be seen that the entire DSF system involves the interactions among different sub-domains in different combinations, namely acoustic-structure, acoustic-acoustic, and acoustic-MPP/MPPA. To explain the modelling procedure and the underlying methodology, an illustration is firstly presented for two neighboring sub-domains. Then, the same procedure is generalized and applied to all sub-systems, which result in an assembled set of system equations for the entire DSF system. In the end, the piecewise calculation scheme is presented to show how the computational burden can be reduced.

2.1 Modelling of Neighboring Sub-systems

Firstly, we consider the interaction between two representative sub-systems coupled over an interface Γ, as shown in Fig. 2, in which the left one is either a structural or an acoustical component whilst the right one is an acoustic component.

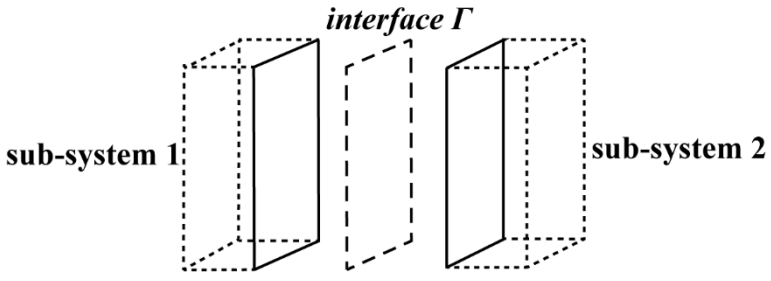

Figure 2 Two sub-systems coupled through an interface.

The physical quantities over Γ are assumed to be coordinately separable. A set of orthonormal functions $\varphi_{rs}(x,y)$, referred to as *Condensation Functions* (CFs), is employed to approximate the velocities and the forces over Γ, as

$$\begin{cases} U^{\alpha}(x,y) = \sum_{r,s} u_{rs}^{\alpha} \varphi_r(x)\varphi_s(y) \\ P^{\alpha}(x,y) = \sum_{r,s} p_{rs}^{\alpha} \varphi_r(x)\varphi_s(y) \end{cases}, \tag{1}$$

where u_{rs}^{α} and p_{rs}^{α} are the amplitudes of the velocity and the sound pressure for each sub-system, denoted by α=1 and α=2, respectively. The acoustic impedance over Γ can be obtained by imposing a prescribed velocity distribution on it. For example, the condensed acoustic impedance between φ_{rs} and φ_{kl} can be written as

$$Z_{kl,rs} = \frac{<\bar{P}_{rs},\varphi_{kl}>}{<U,\varphi_{rs}>} =< \bar{P}_{rs}, \varphi_{kl} >, \tag{2}$$

where $\bar{P}_{rs}$ is the blocked pressure on Γ when the subsystem is subjected to velocity excitation $U(x,y) = \varphi_r(x)\varphi_s(y)$, and $<f, g>$ is a scalar product defined as $\int_{\Omega} f(x,y)g^*(x,y)dS$ with g^* being the complex conjugate of g. Similarly, the condensed mobility between φ_{kl} and φ_{rs} can be written as

$$Y_{rs,kl} = \frac{<\bar{U}_{kl},\varphi_{rs}>}{<P,\varphi_{kl}>} =< \bar{U}_{kl}, \varphi_{rs} >. \tag{3}$$

The velocity continuity and force equilibrium over Γ between the two sub-systems give

$$\begin{cases} U^1 = U^2 \\ P^1 = -P^2 \end{cases}. \tag{4}$$

Then multiplying both sides of Eq. 4 by φ_{rs}, and integrating over Γ, the orthogonality of the CFs alongside Eq. 3 gives:

$$\begin{cases} u_{rs}^1 = u_{rs}^2 \\ p_{rs}^1 = -p_{rs}^2 \end{cases}. \tag{5}$$

Following the procedure as detailed in Ref. [26], the coupled velocity on Γ can be finally expressed as

$$\mathbf{U_c} = -[\mathbf{Z_C^1} + \mathbf{Z_C^2}]^{-1}\mathbf{P_e}, \tag{6}$$

between the two acoustical sub-systems, or

$$\mathbf{U_c} = -[(\mathbf{Y_C^1})^{-1} + \mathbf{Z_C^2}]^{-1}\mathbf{P_e}, \tag{7}$$

between a structural sub-system and an acoustic sub-system, where $\mathbf{Z_C}$ is a matrix containing the condensed impedance of the acoustic sub-system over the interface, $\mathbf{Y_C}$ is a matrix containing the condensed mobility of the structural sub-system over the interface, $\mathbf{U_c}$ and $\mathbf{P_e}$ are the velocity and the blocked pressure induced by the sound source.

The presence of MPP deserves particular attention in terms of modelling. The acoustic impedance of an MPP can be written as,

$$z_{MPP} = r + j\omega m, \tag{8}$$

where ω is the angular frequency and the detailed expressions of r and m can be found in the work of Maa [18]. When the MPP is subject to a grazing flow (for instance, due to the ventilation system), the impedance formula in Eq. 8 could be replaced by the one proposed by Zhang and Cheng [28]. Then, the velocity over the surface of the MPP shall be determined by the acoustic pressure difference across the MPP [29], as

$$u_{MPP} = \frac{p_1 - p_2}{\rho_0 c z_{MPP}}, \tag{9}$$

where ρ_0 is the air density; c the sound velocity; and p_1 and p_2 the acoustic pressure over the MPP surface in cavity C1 and C2, respectively. For the MPPA wall, a backing cavity with a depth D is considered. The backing cavity contributes no additional acoustic resistance to the

MPPA but a relative acoustic reactance $-\cot(\omega D/c)$. As a result, the resulting acoustic impedance of the MPPA over its front surface is given by

$$z_{MPPA} = r + j[\omega m - \cot\left(\frac{\omega D}{c}\right)]. \tag{10}$$

The velocity over the MPPA wall is then determined by the sound pressure p over its surface as,

$$u = \frac{p}{\rho_0 c z_{MPPA}}. \tag{11}$$

Applying the CTF modelling procedure, the acoustic pressure and particle velocity relationship in Eqs. 9 and 11 should be implemented to the corresponding CF coordinate as in Eq. 2 for the MPP modelling.

2.2 Sub-system Assembling and the Piecewise Calculation Scheme

The above modelling procedure is implemented in the entire DSF system depicted in Fig.1. The required condensed impedance or mobility can be separately obtained for the DSF cavity, acoustic room, and the two glasses, respectively. Note all these quantities can be calculated before they are coupled together. In what follows, $\mathbf{Y}_1$ and $\mathbf{Y}_2$ denote the condensed mobility of the outer and inner glasses, respectively. For the condensed impedance, taking $\mathbf{Z}_{23}^{C3}$ as an example, the superscript C3 represents the room and the subscript 23 represents the prescribed velocity at interface 2 and the resulting pressure response at interface 3. The condensed impedance matrices of the MPP screen and the MPPA wall are termed as $\mathbf{Z}_{MPP}$ and $\mathbf{Z}_{MPPA}$, respectively.

Finally, the governing equations of the whole DSF system can be cast into the following form,

$$(\mathbf{Y}_1^{-1} - \mathbf{Z}_{11}^{C1})\mathbf{U}_1 + \mathbf{Z}_{41}^{C1}\mathbf{U}_4 = \mathbf{P}_e, \tag{12}$$

$$(-\mathbf{Z}_{22}^{C2}-\mathbf{Z}_{22}^{C3}+\mathbf{Y}_2^{-1})\mathbf{U}_2+(\mathbf{Z}_{32}^{C2}+\mathbf{Z}_{32}^{C3})\mathbf{U}_3+\mathbf{Z}_{42}^{C2}\mathbf{U}_4+\mathbf{Z}_{52}^{C3}\mathbf{U}_5=\mathbf{0},$$

$$(\mathbf{Z}_{23}^{C2}+\mathbf{Z}_{23}^{C3})\mathbf{U}_2-(\mathbf{Z}_{33}^{C2}+\mathbf{Z}_{33}^{C3})\mathbf{U}_3+\mathbf{Z}_{43}^{C2}\mathbf{U}_4+\mathbf{Z}_{53}^{C3}\mathbf{U}_5=\mathbf{0},$$

$$\mathbf{Z}_{14}^{C1}\mathbf{U}_1+\mathbf{Z}_{24}^{C2}\mathbf{U}_2+\mathbf{Z}_{34}^{C2}\mathbf{U}_3-(\mathbf{Z}_{44}^{C1}+\mathbf{Z}_{44}^{C2}+\mathbf{Z}_{MPP})\mathbf{U}_4=\mathbf{0},$$

$$\mathbf{Z}_{25}^{C3}\mathbf{U}_2+\mathbf{Z}_{35}^{C3}\mathbf{U}_3-(\mathbf{Z}_{55}^{C3}+\mathbf{Z}_{MPPA})\mathbf{U}_5=\mathbf{0},$$

The condensed velocity of the system with MPP can then be solved as

$$\begin{bmatrix}\mathbf{U}_1\\ \mathbf{U}_2\\ \mathbf{U}_3\\ \mathbf{U}_4\\ \mathbf{U}_5\end{bmatrix}=\mathbf{I}_{MPP}^{-1}\begin{bmatrix}\mathbf{P}_e\\ \mathbf{0}\\ \mathbf{0}\\ \mathbf{0}\\ \mathbf{0}\end{bmatrix}, \tag{13}$$

where $\mathbf{I}_{MPP}$ is written as

$$\begin{bmatrix}\mathbf{Y}_1^{-1}-\mathbf{Z}_{11}^{C1} & \mathbf{0} & \mathbf{0} & \mathbf{Z}_{41}^{C1} & \mathbf{0}\\ \mathbf{0} & \mathbf{Y}_2^{-1}-\mathbf{Z}_{22}^{C2}-\mathbf{Z}_{22}^{C3} & \mathbf{Z}_{32}^{C2}+\mathbf{Z}_{32}^{C3} & \mathbf{Z}_{42}^{C2} & \mathbf{Z}_{52}^{C3}\\ \mathbf{0} & \mathbf{Z}_{23}^{C1}+\mathbf{Z}_{23}^{C2} & -\mathbf{Z}_{33}^{C1}-\mathbf{Z}_{33}^{C2} & \mathbf{Z}_{43}^{C2} & \mathbf{Z}_{53}^{C3}\\ \mathbf{Z}_{14}^{C1} & \mathbf{Z}_{24}^{C2} & \mathbf{Z}_{34}^{C2} & -\mathbf{Z}_{44}^{C1}-\mathbf{Z}_{44}^{C2}-\mathbf{Z}_{MPP} & \mathbf{0}\\ \mathbf{0} & \mathbf{Z}_{25}^{C3} & \mathbf{Z}_{35}^{C3} & \mathbf{0} & -\mathbf{Z}_{55}^{C3}-\mathbf{Z}_{MPPA}\end{bmatrix}.$$

If either of the two MPP interfaces is absent, the corresponding $\mathbf{U}_4$ or $\mathbf{U}_5$ becomes zero.

To warrant the convergence of the calculation, the number of CFs used in Eq. 2 should be properly selected and large enough to ensure the convergence of the calculation for the maximum frequency of interest. For the mid-to-high frequency range, the computational time would significantly increase as the matrix size becomes larger. Previous research shows that the number of CFs used can be reduced if the CFs match the wave feature over the coupling interface in the mid-to-high frequency range, which is defined as where the modal overlap factor becomes larger than one [26]. One representative example of the CFs is the complex exponential functions

$$\varphi_{rs}(x,y) = \frac{1}{\sqrt{L_x L_y}} \exp\left(i\frac{2r\pi x}{L_x}\right)\exp\left(i\frac{2s\pi y}{L_y}\right), \tag{14}$$

in which $r \in [0, \pm 1, \pm 2, \ldots, \pm N_x]$, $s \in [0, \pm 1, \pm 2, \ldots, \pm N_y]$. N_x and N_y are two positive integers. The wavelength of $\varphi_{rs}(x,y)$ is defined as:

$$\lambda_{c,rs}(x,y) = \frac{2\pi}{\sqrt{\left(\frac{2r\pi}{L_x}\right)^2 + \left(\frac{2s\pi}{L_y}\right)^2}}. \tag{15}$$

For a targeted frequency band $[f_l, f_h]$ corresponding to a wavelength range $[\lambda_h, \lambda_l]$, it was shown that the condensed velocity $\mathbf{U}_c$ would converge well by only including those dominating terms φ_{rs} which satisfy $\lambda_h < \lambda_{c,rs} < \beta\lambda_l$, with β=1.5 in the calculation. The truncated series is also shown to dominate the condensed impedance matrix and the condensed mobility matrix. Such a treatment was referred to as a piecewise calculation scheme, which will also be used in the subsequent numerical analyses. As a result, the scheme allows a significant reduction in the size of $\mathbf{I}_{MPP}$ so that the computational time can be considerably shortened, as to be substantiated later.

3. Numerical Results and Analyses

In this section, numerical results are presented and analyzed in terms of system response, sound insulation, energy transmission path, and MPP absorption effects. The acoustic properties of the system without MPP is studied first. The two glass panels are assumed to be simply supported, whose thicknesses are 18mm and 12mm for the outer and inner glasses, respectively. The modeling of other plate boundary conditions can be found in the previous work [26]. The outer glass is subject to a diffused incident sound pressure excitation with an amplitude of 0.2Pa. All other geometrical parameters of the system are given in Fig. 1.

3.1 System Response Predictions

The acoustic response in the system is first studied. The predicted Sound pressure level (SPL), calculated by the CTF model at a randomly selected point (0.6, 1.9, 2.9)m inside the room, is shown in Fig. 3a. Recall that the mid-frequency is considered when the modal overlap factor is one which is approximately 220Hz for the present room. Therefore, the calculation for the low-frequency range is conducted using the full CTF calculation, *i.e.* considering only $\lambda_h < \lambda_{c,rs}$. After entering into the mid-frequency range starting from 220Hz, the piecewise calculation scheme is used. The piecewise calculation scheme is implemented within six one-third octave bands centered at 250Hz, 315Hz, 400Hz, 500Hz, 630Hz, and 800Hz, respectively. Similar treatment will be followed throughout this paper.

Comparisons are first made with the Finite Element Method (FEM) for validation purposes using COMSOL. In the model, a zero sound absorption coefficient is assigned to the hard walls of the room. Due to the inherent limitation of the FEM in terms of frequency outreach, only the low-frequency results are compared. It can be seen in Fig. 3a that all the resonance peaks are well predicted despite some discrepancies at some anti-resonance frequencies and the level of some resonance peaks. While the peaks due to the resonances of glasses can be clearly identified in Fig. 3a, those acoustically resonant peaks cannot be simply attributed to the room modes alone. Due to the ventilation opening, the acoustic field in the system is a result of the coupling between the room and the DSF cavity. Generally, the agreement between the two sets of results is more than acceptable.

Figure 3b plots the SPL distribution over a cross-surface at x = 0.6m at 329Hz, which is arbitrarily selected. It can be seen that the detailed acoustic field, as well as the sound pressure contour lines, can be obtained. The established CTF method provides a fine and informative description of the sound pressure distribution over the acoustic room, which allows further analyses and eventually sound field optimizations. It is worth noticing that, in Figs. 3a and 3b, the wealth of information largely exceeds what can be obtained by most commonly used

simulation methods in mid-to-high frequency building acoustics, such as the Statistical Energy Analysis (SEA).

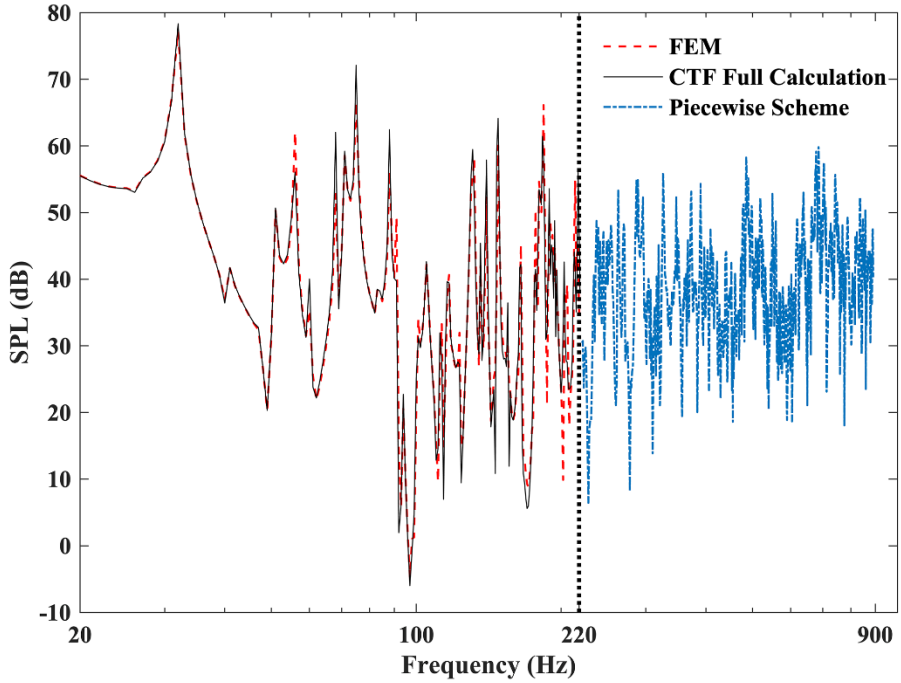

(a)

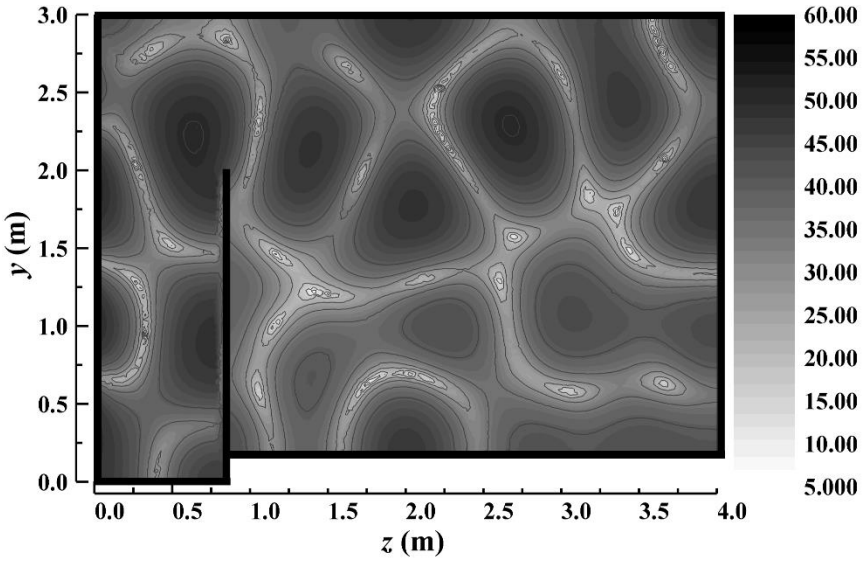

(b)

Figure 3 Acoustic response within the room: (a) SPL at a randomly selected receiving point (0.6, 1.7, 2.4) m, compared with the FEM results in the low-frequency range up to 220Hz; (b) SPL field map at a cut surface x = 0.6 m, at 329Hz.

The mean quadratic velocity (MQV) $\langle U_\alpha \rangle^2$ is commonly used as an indicator for the analyses of vibrating panels, defined as:

$$\langle U_\alpha \rangle^2 = \frac{1}{2S} \iint_S u_\alpha(x,y) u_\alpha^*(x,y) dS_{x,y}, \tag{16}$$

where S is the area of the panel, u is the its velocity, and α is the index of the glass as shown in Fig. 2. However, thanks to the orthogonality of the complex exponential functions, the MQV of the two glass panels can be simply obtained by substituting the velocity vectors in Eq. 13 into Eq. 16, as:

$$\langle U_\alpha \rangle^2 = \frac{1}{2S} \sum_{r,s} |u_{rs}^\alpha|^2 \ . \tag{17}$$

The MQVs of the two glasses are shown in Fig. 4. It can be seen that the velocity difference between the two glasses is relatively small in the very-low-frequency range where the acoustic wavelength is much larger than the depth of the DSF cavity. Particularly for the first few panel resonances, the peak values of the two glasses are almost the same. This can be explained by the double leaf partition model by Fahy [30], in the sense that the two glasses will act as a single one and vibrate in phase when the separation between them is small compared with the acoustic wavelength. For the present depth between the two glasses, this frequency should have been 425Hz where the acoustic pressure within the DSF cavity can be assumed to be uniform. However, the effective depth of the DSF cavity is extensively enlarged due to the ventilation opening and the large dimensions of the room in the back. Therefore, this frequency is lowered to approximately 100Hz as observed in Fig. 4. In the mid-to-high frequency range, the velocity

amplitude of the outer glass becomes significantly larger than that of the inner glass, typically of a few orders of magnitude higher than that of the inner glass.

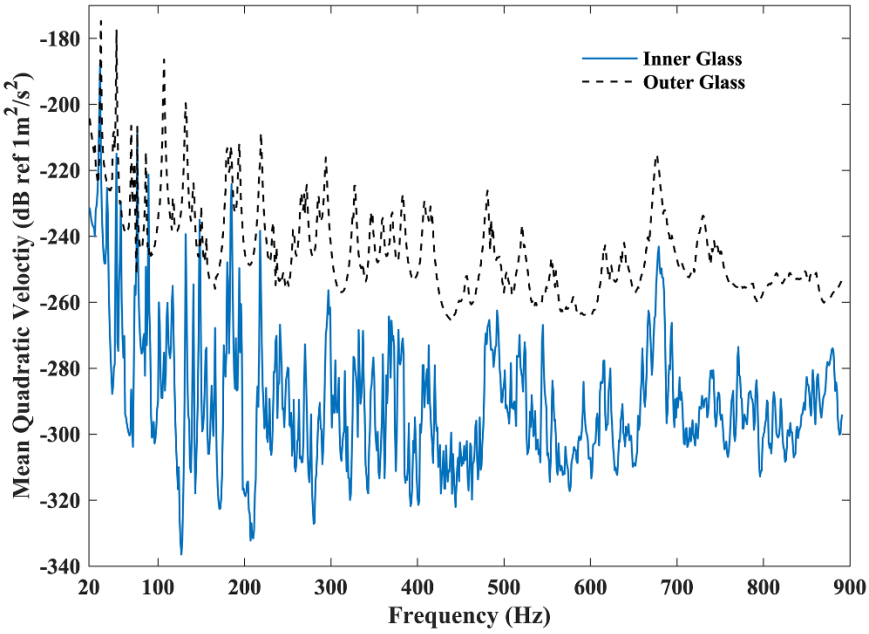

Figure 4 CTF prediction results: mean quadratic velocities of the two glasses.

To show the efficiency improvement by the piecewise calculation scheme, a size reduction ratio R of matrix $\mathbf{I}_{MPP}$ in Eq. 13 is defined as

$$R = \frac{N_f - N_p}{N_f} \times 100\% \tag{18}$$

where N_f and N_p are the number of elements in $\mathbf{I}_{MPP}$ in full and piecewise calculation schemes, respectively. R is tabulated in Table 1 for different configurations and frequency bands. It can be seen the piecewise calculation scheme leads to a significant reduction in the size of the matrix to be maneuvered, especially for the mid-to-high frequency range. Additionally, the improvement is more evident when the number of involved coupling interfaces increases.

Table 1 Matrix size reduction ratio by the piecewise calculation scheme compared with the full CTF calculation

Size Reduction Ratio (%)	One-third Octave Centre Frequency (Hz)				
	400	500	630	800	1000
Empty Room	27.4	38.5	41.3	43.0	39.1
MPPA Wall	30.3	42.2	42.5	43.9	42.4
MPP Screen	32.5	42.3	42.9	44.1	43.4
Wall and Screen	34.5	43.1	43.6	45.8	45.3

3.2 Analyses on the sound transmission paths

For the general noise control purposes, it is vital to identify the dominant energy transmission path in a complex system. In the present case, to further understand how the sound energy is transmitted into the room, the sound power transmitted through two possible paths, *i.e.* ventilation opening and the inner glass, are compared. The transmitted sound power level L_w is obtained by integrating the sound intensity over the ventilation opening and the inner glass, respectively as

$$L_w = 10\log_{10}\left(\frac{\int_S I_z dS}{10^{-12}}\right), \tag{19}$$

where I_z is the *z*-direction component of the sound intensity and *S* is the area of either the inner glass or the ventilation opening. Because L_w is generally positive, we use L_w to represent the power going into the room (positive I_z) and $-L_w$ to represent the power going out of the room (negative I_z). Figure 5a shows the power transmitted via the inner glass. The upper half of the figure (y>0) shows the power flows into the room while the lower half (y<0) presents that out of the room. While acoustic energy is mostly generated by the inner glass vibration, thus injecting positive power into the room, it can also be noticed that at some frequencies, the acoustic power can flow out of the room into the inner glass. On the contrary, the sound energy

generally flows into the room via the ventilation opening in a very predominant way, except for a few very narrow bands at low frequencies, as shown in Fig. 5b.

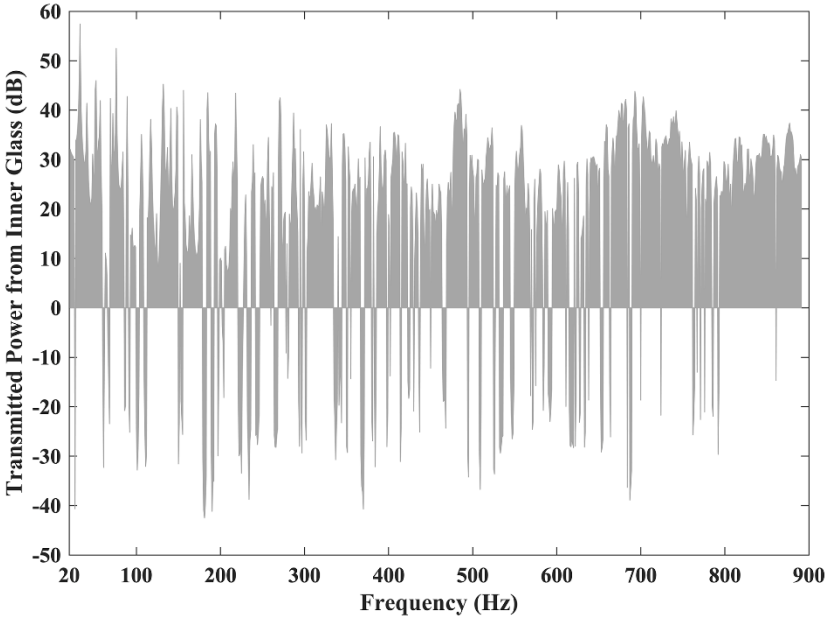

(a)

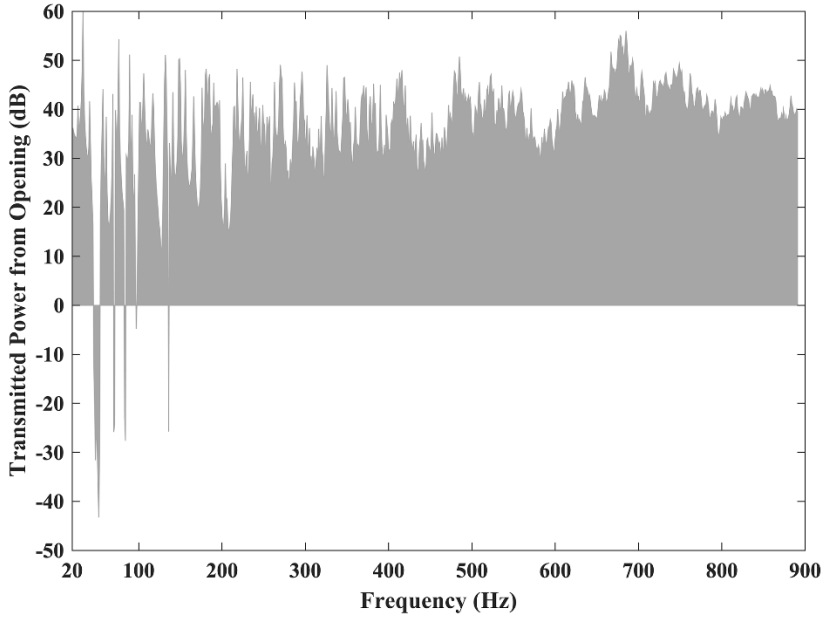

(b)

Figure 5 Transmitted acoustic power into the room via: (a) Inner glass; (b) Ventilation opening.

Due to its dominant role in sound energy transmission, the transmissibility of the ventilation opening is further analyzed with respect to its opening size in the y-direction. For quantifications, in this paper the sound reduction index (SRI) is defined as

$$\text{SRI} = L_{wo} - L_{wi} - L_{wv}, \tag{20}$$

where L_{wo}, L_{wi}, and L_{wv} are the sound power transmitted through the outer glass, inner glass, and ventilation opening, respectively. In the analyses, the total height of the inner glass and the opening is kept constant, *i.e.* the height of the inner glass reduces as the size of the opening increases. Other dimensions and boundary conditions remain the same as before. Figures 6a and 6b present the SRI with respect to different opening sizes at two arbitrarily selected frequencies, *i.e.* 500 and 600Hz, respectively. It can be observed that the SRI firstly fluctuates while taking a slightly increasing trend as long as the opening size is larger than the half wavelength of the acoustic waves, as shown by the vertical dash line. This can be attributed to the complex modal interaction between the DSF cavity and the room, which was identified as a "strong coupling" case in our previous work [27]. The sound transmission is dominated by the opening in this region. When the opening size approaches or becomes smaller than the half acoustic wavelength, the SRI sharply increases due to the vanishing of higher order waves along the y-direction. Presumably, the increasing trend of SRI will continue until the sound transmission is taken over by the vibration of the inner glass if the latter is significant enough, which depends on the glass configurations. Therefore, to prevent noise from transmitting through the ventilation opening at a given frequency, its opening size should be kept below the corresponding half acoustic wavelength.

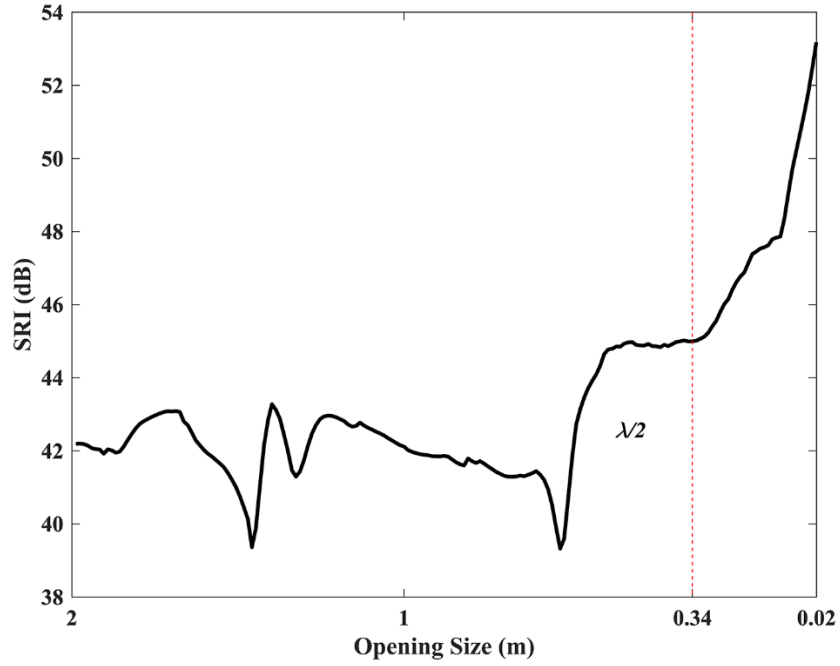

(a)

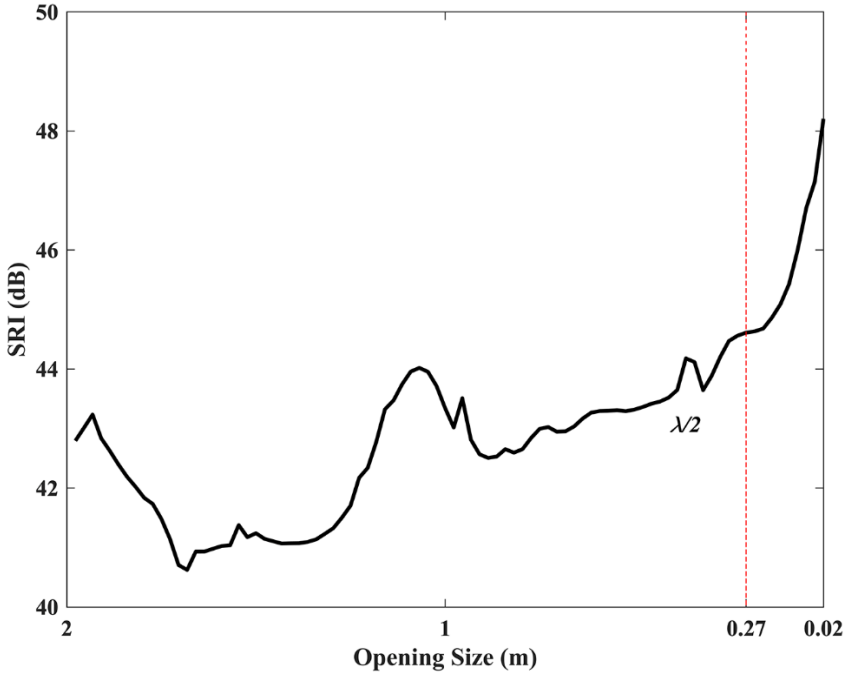

(b)

Figure 6 The influence of the opening size on the SRI at: (a) 500Hz; (b) 630Hz.

3.3 Applications of MPPs

The noise control performance of using MPPs in two different settings and the corresponding *in-situ* sound absorption behaviors are investigated in this section. According to the above analyses, efforts are put on the frequencies where the half acoustic wavelength is smaller than the size of ventilation opening, which is 212Hz in the present case. The parameters of the MPP used are listed in Table 2. For the MPPA wall, the sound absorption coefficient can be estimated by the formula obtained by Maa [18], which is shown in Fig. 7. It can be seen the effective sound absorption band properly covers the concerned frequency range up to 1000Hz.

Table 2 Parameters of the Micro-perforated Panel and the backing cavity for MPPA

Hole diameter	Panel thickness	Perforation ratio	Depth of backing cavity for MPPA
0.1mm	0.1mm	0.1%	0.1m

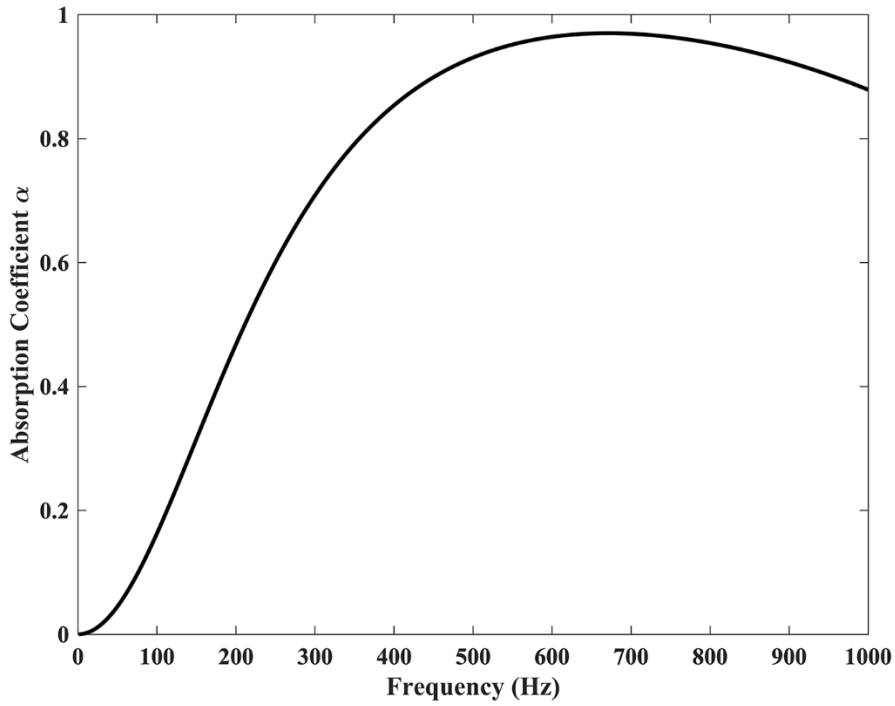

Figure 7 Absorption coefficient of the MPP.

Figure 8 shows the SPLs inside the room, at the same point as the one used in Fig. 3, corresponding to three cases: without MPP, with MPPA wall only and with both MPPA wall and MPP screen. The dotted line represents the SPL without MPP. Comparison with the case of the MPPA wall shows a significant reduction of the SPL inside the room, especially in terms of suppressing the peaks, amounting to an average of 10 dB reduction. Note these peaks are predominantly due to the resonances of the acoustic room, and those of the inner glass to a much less extent. Interestingly enough, it can be noticed that MPPA fails at some particular peaks, for example, the one at 220Hz. These peaks are identified as the resonance frequencies of the inner glass. Such deficiencies can be alleviated by adding an MPP screen inside the DSF cavity, as evidenced by the real line in Fig. 8. It can be observed that the MPP screen can further reduce the SPL on the basis of the existing MPPA wall, both at resonance and non-resonance frequencies, including where the MPPA wall is ineffective. Obviously, using simultaneously the MPPA wall and the MPP screen lead to the best noise reduction performance among the three cases.

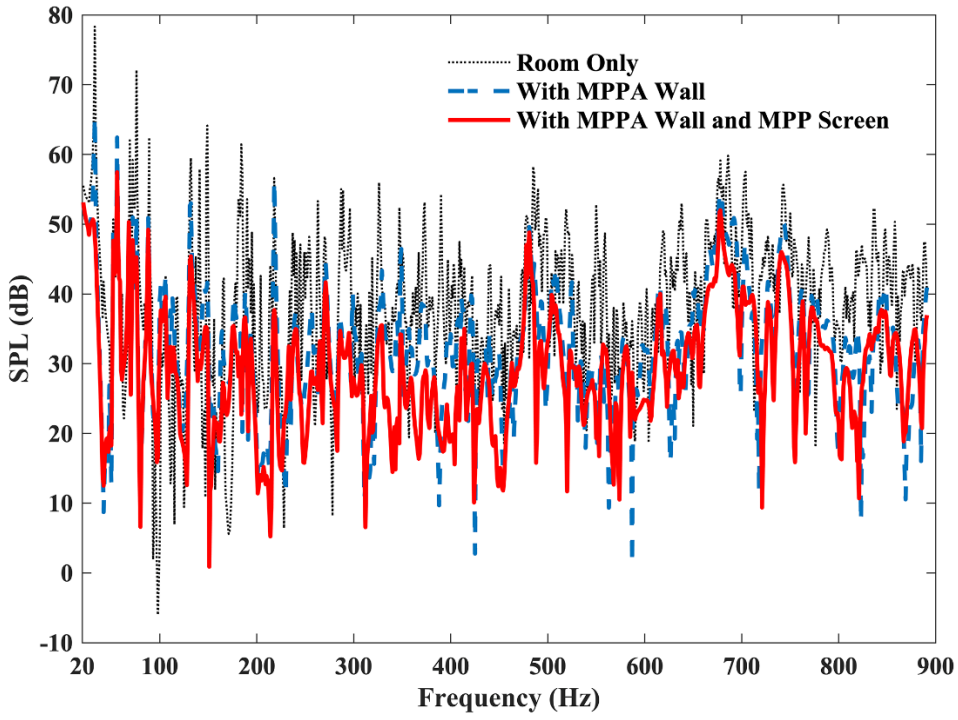

Figure 8 SPL obtained from different MPP arrangements at (0.6, 1.9, 2.9)m.

The volume averaged SPL within one-third octave bands are shown in Fig. 9. Besides the three cases considered in Fig. 8, the SPL prediction with only MPP screen is also included for a more comprehensive comparison. It can be observed that generally, the MPPA wall outperforms the MPP screen by offering approximately 5-10 dB more sound reduction when they are separately used. It is also worth noticing that, for example within the 125Hz band, no or little SPL reduction is observed when the MPP screen or the MPPA wall is separately used. However, if the two arrangements are used together, an extra sound reduction can be achieved. This implies that the performance of the MPP sound absorption cannot be predicted by simply superposing the results from individual elements. It also alludes to the fact that the deployment of multiple sound absorption measures, exemplified by MPPs in the present context, would alter the acoustic field so that the individual performance could be affected. Meanwhile, this shows there is a considerable room for properly designing and optimizing the settings of the MPPs and their coupling with the rest of the vibroacoustic system to maximize the noise reduction, which inevitably needs to be conducted case by case with the help of an effective simulation tool.

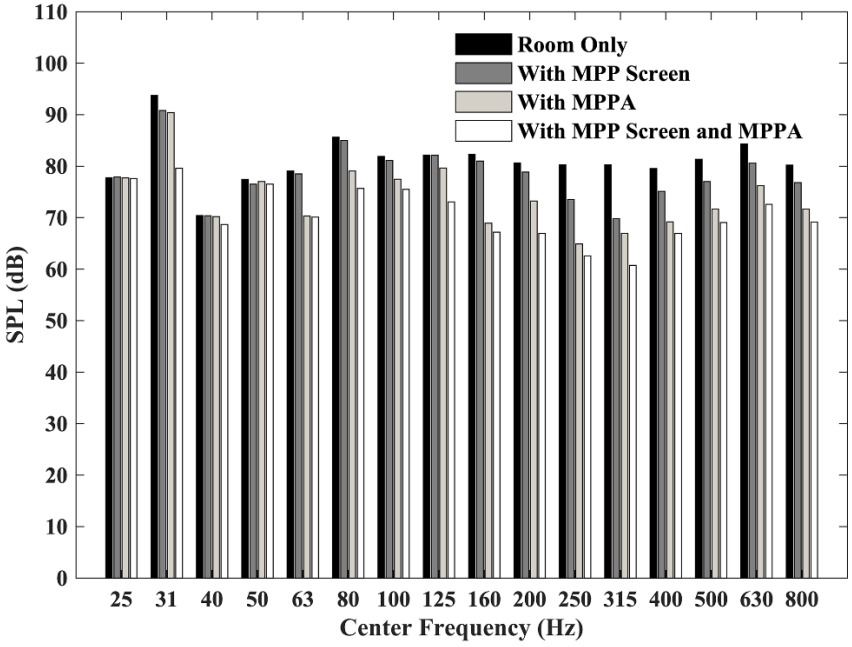

Figure 9 Volume averaged SPL within the room, in one-third octave bands.

Analyses are conducted to further demonstrate the underlying sound absorption mechanisms of the MPPA wall and MPP screen, as well as to understand their mutual interaction in such a complex acoustic environment. Figure 10a shows the SPL distribution over a cutting surface inside the acoustic room, located at x = 0.6m, only with the MPPA wall at 329Hz. To better compare the differences in SPL, all cloud pictures in Fig. 10 use the same color scale. Comparing Fig. 10a with Fig. 3b shows that the deployment of the MPPA wall will not only reduce the SPL within the room but also change the sound pressure distribution within the system including the DSF cavity. With an MPP screen added inside the DSF cavity (Fig. 10b), it can be seen that different from the MPPA wall, the MPP screen interacts more effectively with its surrounding acoustic environment and provides effective sound absorption when a pressure difference exists across the MPP. In the present case, this effect can be evidenced by the pressure difference across the MPP in the middle portion of the screen, roughly ranging from y = 1m to y = 2m. Therefore, even without the backing cavity, the MPP screen can still provide appreciable sound absorption based on this non-locally reacting and fully coupled working mechanism. To further assess this, Fig. 10c shows the sound intensity distribution over the cutting surface. It can be seen that the sound power indeed flows into the MPP screen, which illustrates the occurrence of sound absorption through the MPP screen.

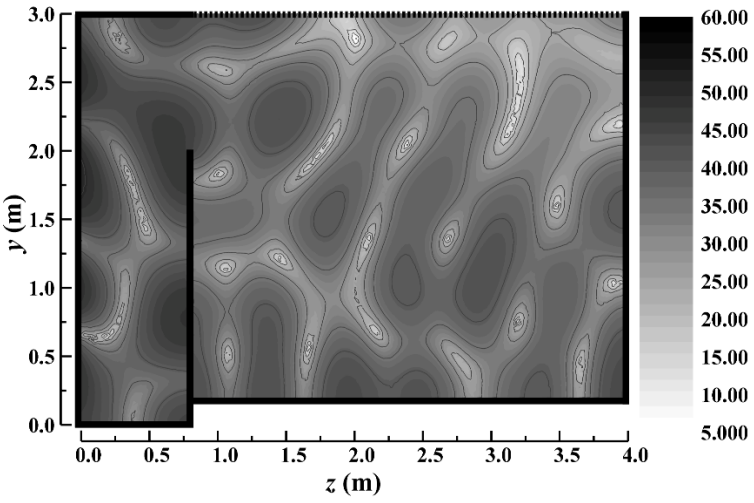

(a)

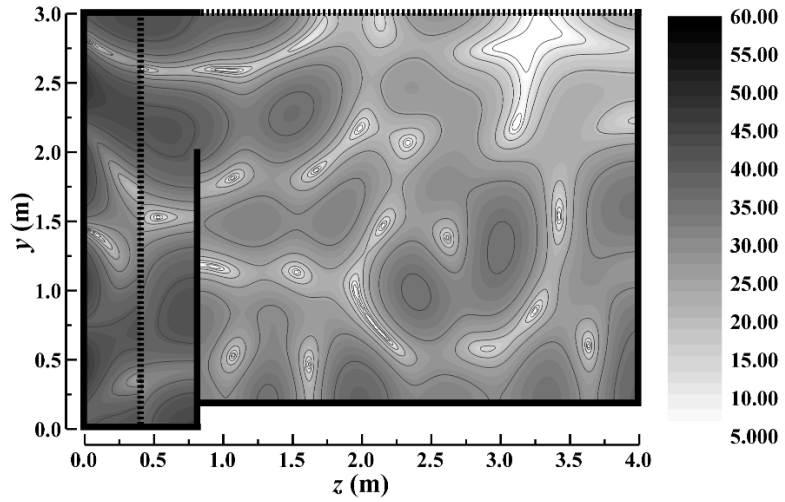

(b)

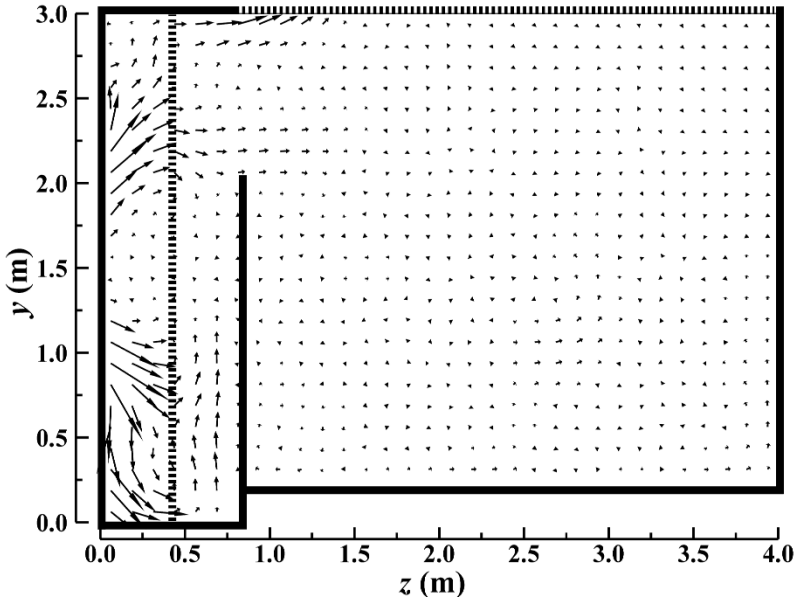

(c)

Figure 10 Sound field distribution at the cutting surface x = 0.6m, 329Hz: (a) SPL mapping with MPPA; (b) SPL mapping with MPPA and MPP screen; (c) Sound intensity with MPPA and MPP screen.

To further quantify the sound absorption performance of the MPP screen, an equivalent absorption coefficient is defined as

$$\alpha_{eq} = \int_S \frac{I_{z1} - I_{z2}}{I_{z1}} dS, \tag{21}$$

where I_{z1} and I_{z2} are the *z*-component of the sound intensity on both sides of the MPP screen, respectively. α_{eq}, with and without the MPPA wall are plotted in Fig. 11. It can be observed that α_{eq} is generally slightly larger when the MPPA wall exists, consistent with the observations from Fig. 8. On the other hand, regardless of the existence of the MPPA wall, the frequency variations of α_{eq} exhibits complex patterns. An interesting question is whether α_{eq} can be approximately predicted by Eq. 10. Considering the DSF cavity as a backing cavity, an approximated absorption coefficient curve can be calculated using Eq. 10 and plotted in Fig. 11. It can be observed that, if omitting details, the general variation trend of α_{eq} vaguely shows a certain degree of resemblance with the classical sound absorption curve of an MPPA in terms of amplitude envelop, but slightly shifted towards lower frequencies. This can be attributed to the reduction in the equivalent stiffness of the cavity, as a result of an increase in the effective depth of the DSF cavity due to the ventilation opening and its connection with the acoustic cavity behind. By scrutinizing the detailed variation of α_{eq}, it can be concluded that the complex acoustic field, to which the MPP screen is exposed, creates a complex yet favorable working environment for MPP, thus promoting its *in-situ* sound absorption, which cannot be exactly predicted by conventional sound absorption formula. Although a rough estimation is possible based on the common understanding of the working principle of the MPP sound absorption, meticulous design and optimization are needed to cater for a particular application with the aid of an effective simulation tool like the one developed in this paper.

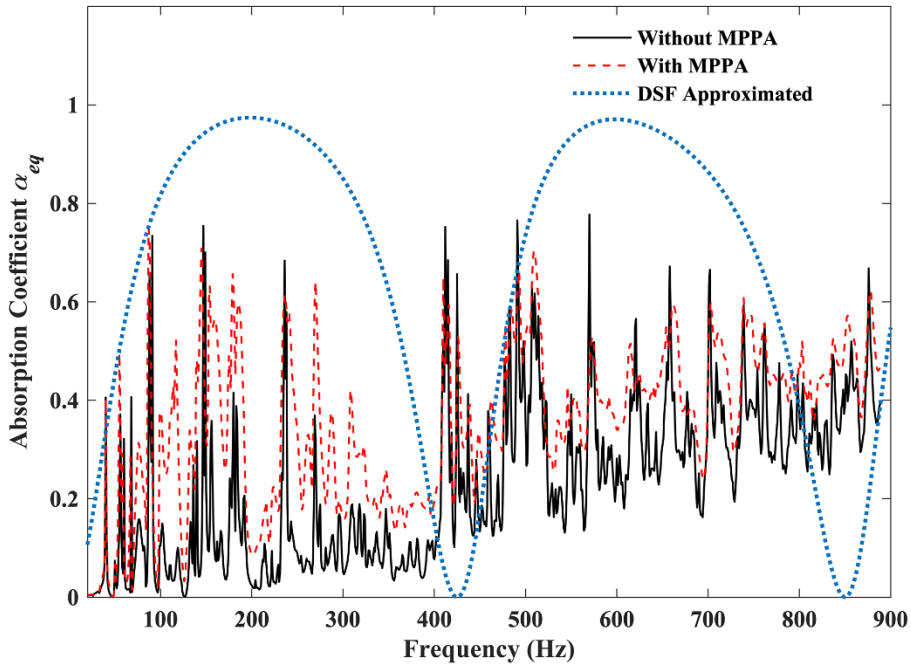

Figure 11 Equivalent absorption coefficient of the MPP screen and comparison of an MPPA.

4. Conclusions

In this paper, a Condensed Transfer Function method is adapted and proposed to deal with the acoustic prediction of a simplified DSF system. Through integrating typical MPP-based sound absorption treatments, dominant noise transmission paths through the system, as well as the *in-situ* sound absorption behaviors of different sound absorption arrangements, are explored.

The proposed modeling methodology has been shown to allow efficient and flexible handling of a typical DSF acoustic system by providing a fine and detailed description of major vibro-acoustic metrics of this complex vibro-acoustic system with a relatively large dimension. With the adoption of a piecewise calculation scheme, numerical prediction can reach the so-called mid frequency range where the system exhibits rich dynamics and a high modal density.

It is shown that noise can be transmitted into the acoustic room in a typical DSF system through both air-borne (through the ventilation opening of the inner glass panel) and structure-borne (through the vibration of the inner galls panel) paths. Their relative dominance level,

however, depends on the system configuration. In general, the sound insulation of the DSF system is highly dependent on the size of the ventilation opening. The SRI can be significantly compromised when the size of the ventilation opening of the inner glass exceeds half acoustic wavelength at sufficiently high frequencies. The use of MPPs, either as an absorbing wall or a screen inside the DSF cavity, is proved to be an efficient way to reduce the SPL within the room. While an MPPA provides efficient sound energy absorption based on the well-known locally reacting behavior, the MPP screen also offers appreciable sound absorption by benefiting from its non-locally reacting interaction with the surrounding acoustic environment inside the DSF cavity, provided a favorable sound pressure difference can be generated across the MPP screen. This can be achieved through proper design of the system configuration, for example through the use of MPPA to alter the sound distribution inside the DSF cavity. As a result, extra sound reduction inside the acoustic room can be achieved. This, of course, would need an efficient, flexible and versatile numerical model such as the one presented in the present work to guide the design.

Reference

[1] C.M. Mak and Z. Wang, "Recent advances in building acoustics: An overview of prediction methods and their applications," Building and Environment **91**, 118-126 (2015).

[2] J.M. Navarro and J. Escolano, "Simulation of building indoor acoustics using an acoustic diffusion equation model," Journal of Building Performance Simulation **8**(1), 3-14 (2015).

[3] K. Orehounig and A. Mahdavi, "Performance evaluation of traditional bath buildings via empirically tested simulation models," Journal of Building Performance Simulation **4**(1), 63-74 (2011).

[4] H. Kuttruff, *Room acoustics*. 2016: Crc Press.

[5] M. Hornikx, C. Hak, and R. Wenmaekers, "Acoustic modelling of sports halls, two case studies," Journal of Building Performance Simulation **8**(1), 26-38 (2015).

[6] A. Arjunan, C.J. Wang, K. Yahiaoui, D.J. Mynors, T. Morgan, V.B. Nguyen, and M. English, "Development of a 3D finite element acoustic model to predict the sound reduction index of stud based double-leaf walls," Journal of Sound and Vibration **333**(23), 6140-6155 (2014).

[7] A. Santoni, P. Bonfiglio, J.L. Davy, P. Fausti, F. Pompoli, and L. Pagnoncelli, "Sound transmission loss of ETICS cladding systems considering the structure-borne transmission via the mechanical fixings: Numerical prediction model and experimental evaluation," Applied Acoustics **122**, 88-97 (2017).

[8] C. Diaz-Cereceda, J. Poblet-Puig, and A. Rodriguez-Ferran, "The finite layer method for modelling the sound transmission through double walls," Journal of Sound and Vibration **331**(22), 4884-4900 (2012).

[9] D. Urbán, N.B. Roozen, P. Zaťko, M. Rychtáriková, P. Tomašovič, and C. Glorieux, "Assessment of sound insulation of naturally ventilated double skin facades," Building and Environment **110**, 148-160 (2016).

[10] J.M. Navarro, J. Escolano, and J.J. Lopez, "Implementation and evaluation of a diffusion equation model based on finite difference schemes for sound field prediction in rooms," Applied Acoustics **73**(6-7), 659-665 (2012).

[11] P. Luizard, J.D. Polack, and B.F.G. Katz, "Sound energy decay in coupled spaces using a parametric analytical solution of a diffusion equation," Journal of the Acoustical Society of America **135**(5), 2765-2776 (2014).

[12] S. Kurra, "Comparison of the models predicting sound insulation values of multilayered building elements," Applied Acoustics **73**(6-7), 575-589 (2012).

[13] S. Nakanishi, M. Yairi, and A. Minemura, "Estimation method for parameters of construction on predicting transmission loss of double leaf dry partition," Applied Acoustics **72**(6), 364-371 (2011).

[14] M.E. Delany and E.N. Bazley, "Acoustical properties of fibrous absorbent materials," Applied Acoustics **3**(2), 105-116 (1970).

[15] J.P. Groby, C. Lagarrigue, B. Brouard, O. Dazel, V. Tournat, and B. Nennig, "Using simple shape three-dimensional rigid inclusions to enhance porous layer absorption," Journal of the Acoustical Society of America **136**(3), 1139-1148 (2014).

[16] R. del Rey, J. Alba, J.P. Arenas, and V.J. Sanchis, "An empirical modelling of porous sound absorbing materials made of recycled foam," Applied Acoustics **73**(6-7), 604-609 (2012).

[17] D.-Y. Maa, "Theory and design of microperforated panel sound-absorbing constructions," Scientia Sinica **18**(1), 55-71 (1975).

[18] D.-Y. Maa, "Potential of microperforated panel absorber," Journal of the Acoustical Society of America **104**(5), 2861-2866 (1998).

[19] C. Yang, L. Cheng, and Z.Y. Hu, "Reducing interior noise in a cylinder using micro-perforated panels," Applied Acoustics **95**, 50-56 (2015).

[20] Z.Y. Hu, C. Yang, and L. Cheng, "Acoustic resonator tuning strategies for the narrowband noise control in an enclosure," Applied Acoustics **134**, 88-96 (2018).

[21] G. Yu, D. Li, and L. Cheng, "Effect of internal resistance of a Helmholtz resonator on acoustic energy reduction in enclosures," Journal of the Acoustical Society of America **124**(6), 3534-43 (2008).

[22] J.P. Groby, C. Lagarrigue, B. Brouard, O. Dazel, V. Tournat, and B. Nennig, "Enhancing the absorption properties of acoustic porous plates by periodically embedding Helmholtz resonators," Journal of the Acoustical Society of America **137**(1), 273-280 (2015).

[23] M. Aucejo, L. Maxit, N. Totaro, and J.L. Guyader, "Convergence acceleration using the residual shape technique when solving structure–acoustic coupling with the Patch Transfer Functions method," Computers & Structures **88**(11-12), 728-736 (2010).

[24] X. Yu, L. Cheng, and J.L. Guyader, "Modeling vibroacoustic systems involving cascade open cavities and micro-perforated panels," Journal of the Acoustical Society of America **136**(2), 659-70 (2014).

[25] J.-D. Chazot and J.-L. Guyader, "Transmission loss of double panels filled with porogranular materials," The Journal of the Acoustical Society of America **126**(6), 3040-3048 (2009).

[26] Z.Y. Hu, L. Maxit, and L. Cheng, "Piecewise convergence behavior of the condensed transfer function approach for mid-to-high frequency modelling of a panel-cavity system," Journal of Sound and Vibration **435**, 119-134 (2018).

[27] Z.Y. Hu, L. Maxit, and L. Cheng, "Mid-to-high frequency piecewise modelling of an acoustic system with varying coupling strength," Mechanical Systems and Signal Processing **134**, (2019).

[28] X. Zhang and L. Cheng, "Acoustic impedance of micro-perforated panels in a grazing flow," The Journal of the Acoustical Society of America **145**(4), 2461-2469 (2019).

[29] C. Yang and L. Cheng, "Sound absorption of microperforated panels inside compact acoustic enclosures," Journal of Sound and Vibration **360**, 140-155 (2016).

[30] F.J. Fahy and P. Gardonio, *Sound and structural vibration: radiation, transmission and response*. 2007: Academic press.